Dynamics of the optical spin Hall effect

Daniel Schmidt,[1] Bernd Berger,[1] Manfred Bayer,[1,2] Christian Schneider,[3] Martin Kamp,[3] Sven Höfling,[3,4] Evgeny Sedov,[5,6] Alexey Kavokin,[6,7,8] and Marc Aßmann[1]

[1]*Experimentelle Physik 2, Technische Universität Dortmund, D-44221 Dortmund, Germany*
[2]*A. F. Ioffe Physical-Technical Institute, Russian Academy of Sciences, Saint Petersburg 194021, Russia*
[3]*Technische Physik, Universität Würzburg, 97074 Würzburg, Germany*
[4]*SUPA, School of Physics and Astronomy, University of St Andrews, St Andrews, KY16 9SS, United Kingdom*
[5]*Department of Physics and Applied Mathematics, Vladimir State University, Gorky Strasse 87, 600000 Vladimir, Russia*
[6]*School of Physics and Astronomy, University of Southampton, SO17 1NJ Southampton, England, United Kingdom*
[7]*Spin Optics Laboratory, Saint Petersburg State University, Ul'anovskaya 1, Peterhof, Saint Petersburg 198504, Russia*
[8]*CNR-SPIN, Viale del Politecnico 1, I-00133 Rome, Italy*

(Received 2 June 2017; revised manuscript received 31 July 2017; published 24 August 2017)

We study the time evolution of the optical spin Hall effect, which occurs when exciton polaritons undergo resonant Rayleigh scattering. The resulting spin pattern in momentum space is quantified by calculating the degree of circular polarization of the momentum space image for each point in time. We find the degree of circular polarization performing oscillations, which can be described within the framework of the pseudospin model by Kavokin *et al.* [A. Kavokin, G. Malpuech, and M. Glazov, Phys. Rev. Lett. **95**, 136601 (2005)].

DOI: 10.1103/PhysRevB.96.075309

I. INTRODUCTION

Exciton polaritons, which are composite bosons arising from strong coupling between quantum well (QW) excitons and cavity photons, play an important role in the rapidly developing research field of spin optronics or semiconductor spin optics. Due to their excitonic component, polaritons interact with each other, whereas the photonic component allows much faster propagation compared to bare excitons. The resulting optical reconfigurability of exciton polaritons in semiconductor microcavities therefore is a striking feature which potentially allows one to realize all-optical devices for information technology. A lot of phenomena related to polariton switching and propagation recently have been investigated experimentally, such as polarization dependent switching [1], all-optical logic gates [2,3], and bistable [4] and multistable [5,6] switching of polariton reservoirs. Also the propagation dynamics of exciton polaritons has been studied extensively [7–10].

One possible way of creating polariton flows is by use of the nonresonant optical excitation energetically far above the resonant cavity mode. Using tailored spatial excitation patterns, all-optical flow control [11], polariton amplification [12], and advanced momentum control [13] have been demonstrated successfully. Polariton flows can also be created by resonant optical excitation of the lower polariton branch (LPB). The momentum direction of the in-plane propagation is then directly controlled by the incidence angle of the excitation beam. When a polariton flow is directed onto a defect in the sample, such as a structural defect or impurity, a scattering ring builds up in momentum space due to elastic scattering [14–16].

The polaritons inherit fundamental properties from their constituents. Heavy-hole excitons are characterized by angular momentum projections on the QW growth axis that take values ± 1 and ± 2. The so-called dark excitons with ± 2 projections are optically inactive and in most cases their influence on light-matter interaction processes can be safely neglected. At the same time, the bright excitons with angular momentum projections ± 1 are allowed to couple with cavity photons of two opposite (right and left) circular polarizations, respectively, and form a polariton spin doublet state. To describe this doublet, we can introduce the pseudospin vector $\mathbf{S}$. Its behavior in time is governed by the built-in effective magnetic fields of different origin.

In this paper, we investigate the dynamics of the optical spin Hall effect (OSHE), which takes place due to the elastic-scattering processes in a spin-polarized gas of propagating exciton polaritons [17]. The OSHE describes the formation of spin currents due to an effective magnetic field, which is induced by the longitudinal-transverse (LT) splitting of the cavity photon modes. In the passage of time characteristic anisotropic spin patterns form in the momentum space. Recent works reported on the observation of the spin currents [18,19] and anisotropy effects [20] in both real and momentum space. Further, a nonlinear analog of the OSHE was demonstrated [21]. Even the influence of an external magnetic field was examined theoretically [22]. All these works demonstrate the control of polariton spin currents, especially in the time-integrated momentum space.

In the present paper we aim for gaining control over the spin currents in the time domain. Therefore, we perform time-resolved measurements of the momentum space of elastically scattered polaritons. We identify the spin currents induced by the OSHE and experimentally study their time dependence. The measured temporal behavior can be well reproduced utilizing the pseudospin model [17,23].

II. EXPERIMENT

Our sample is a planar GaAs λ cavity with six $In_{0.1}Ga_{0.9}As$ quantum wells placed at the central antinodes of the confined light field and 26 top and 30 bottom GaAs/AlAs Distributed Bragg reflector (DBR) layer pairs. The Rabi splitting amounts to about 6 meV. The measurements are performed at the detuning $\delta = E_{\mathrm{cav}}(k_{||}{=}0) - E_{\mathrm{exc}}(k_{||}{=}0)$ of -5.3 meV. We excite the sample resonant to the TM mode of the lower polariton

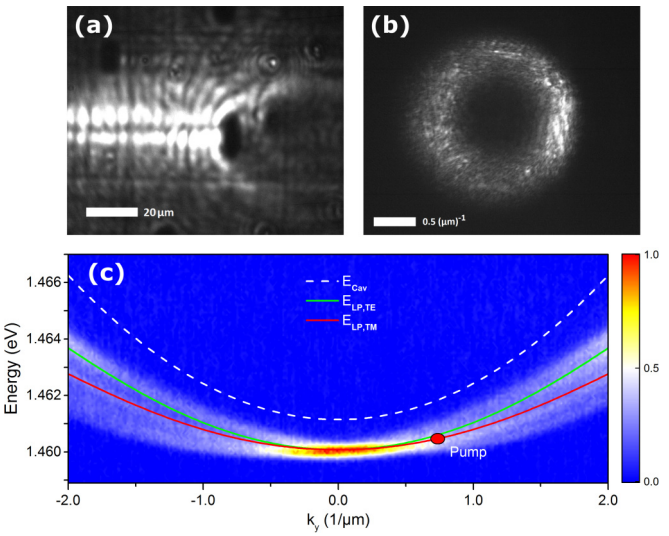

FIG. 1. (a) Real-space image of resonant scattering. (b) Corresponding momentum space image of resonant scattering. (c) Dispersion probed by nonresonant excitation with $k = 0$. The TE-TM splitting is clearly visible. The pump configuration used when performing resonant scattering experiments is marked with the red dot. The polarization is matched to the TM mode of the lower polariton branch. The entrance slit of the spectrometer is aligned central to the emission spot.

branch with a pulsed picosecond Ti:Sa laser centered at 848.86 nm (1.46060 eV) and create polaritons with an in-plane wave vector of $k_{||} = 0.73\,(\mu\text{m})^{-1}$. The power is 15 mW with a Gaussian spot diameter of 20 μm. Using a cold-finger continuous flow cryostat the measurements are performed at 15 K. For spectral analysis the signal is sent to a 500-mm monochromator equipped with a nitrogen cooled CCD camera. A Hamamatsu streak camera with S-20 photocathode allows for time-resolved measurements, for which an interference filter ensures that only the emission from the LPB is detected.

See Fig. 1 for the intermediate images of the real space (a) and momentum space (b). For comparison the whole dispersion of the polaritons following nonresonant excitation is shown in Fig. 1(c). In the momentum space for certain sample positions a typical scattering ring appears, due to the elastic Rayleigh scattering of exciton polaritons by sample inhomogeneities or defects. Under resonant excitation and nonzero incidence pronounced defect scattering can be observed [see Fig. 1(a)]. The propagating exciton polaritons undergo self-interference resulting in a typical standing-wave pattern around the defect.

Here we temporally resolve this scattering process. Further, the distribution of spins is investigated to evaluate the pseudospin precession due to the OSHE. Therefore we polarize the incident beam linearly and direct it onto the sample under an aligned angle to resonantly excite the TM mode of the LPB.

Since we want to capture the full time evolution of the momentum space distribution, we record single frames with k_x-t information and merge them. To do so, we move the endmost lens in front of the streak camera stepwise to shift the momentum space image along the k_y direction, perpendicular to the entrance slit of the streak camera [24]. Thereby we

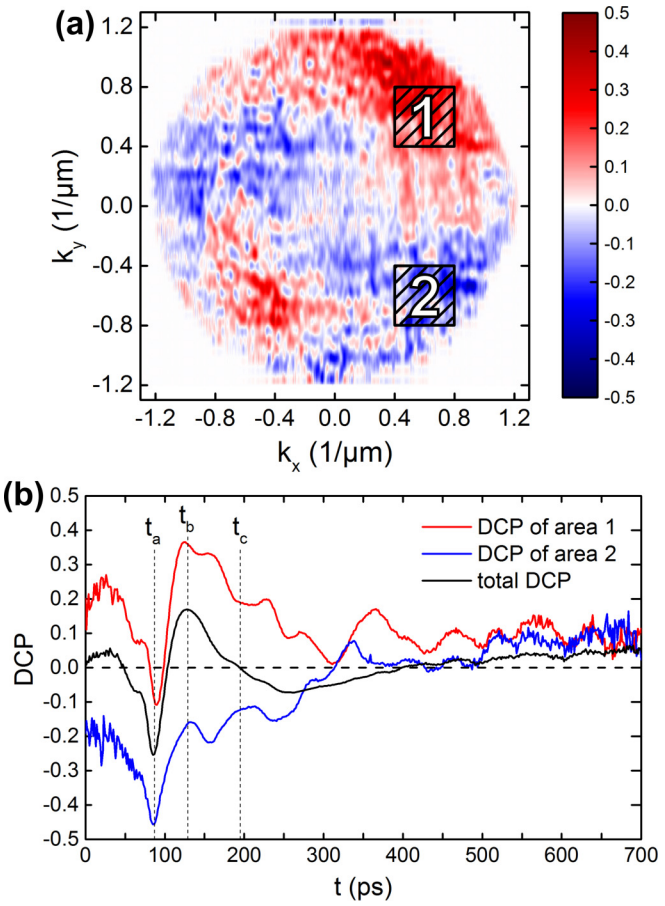

FIG. 2. (a) Time integrated image of the DCP in momentum space with marked areas 1 and 2. (b) Time evolution of the DCP in selected areas 1 and 2. The recorded time frame starts at $t_0 = 0$ prior to the incidence of the excitation pulse.

incrementally capture the full time evolution of the scattering ring in momentum space for both σ^+ and σ^- polarization [25].

III. RESULTS

From the recorded data, the degree of circular polarization (DCP) ρ_c can be extracted at each k_x-k_y point in momentum space for any point in time using

$$\rho_c = \frac{I_{\sigma^+} - I_{\sigma^-}}{I_{\sigma^+} + I_{\sigma^-}}. \tag{1}$$

We integrate the data over time and calculate the DCP to verify the typical pseudospin pattern of the OSHE. This is shown in Fig. 2(a). To reveal the time evolution of the DCP two areas are selected at angles of $+45°$ and $-45°$ with respect to the direction of the pump. Results for the chosen areas are shown in Fig. 2(b), where oscillations with opposite DCP signs can be observed. This resembles the behavior [17] originally predicted. However, some striking deviations can be observed. First, the DCP in both areas initially drops to negative values, which we attribute to a small, unavoidable initial polarization of the pump when focused onto the sample. Second, the DCP does not drop to zero during the initial oscillations in the interval of 150–300 ps. An intuitive explanation for this is the

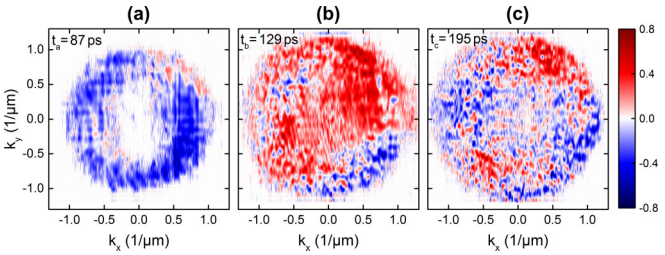

FIG. 3. DCP of momentum space at selected points in time corresponding to the marked points in time of Fig. 2(b).

superposition of multiple oscillations with different frequency. This behavior can be understood in terms of the pseudospin model, which will be discussed in depth in Sec. IV.

Beyond the time evolution of characteristic points of the momentum space, some snapshots at certain points of interest in time merit further investigation, as shown in Fig. 2(b). t_a coincides with the initial drop to a negative DCP. t_b denotes the point in time with maximal positive DCP. Finally, t_c is selected such that the overall DCP of the total momentum space vanishes although in both areas the DCP is nonzero. The related momentum space snapshots are shown in Fig. 3. The first snapshot at $t_a = 87$ ps shows a negative DCP everywhere on the scattering ring. Since no precession is observable, we conclude that this is the time of excitation when resonant Rayleigh scattering without loss of polarization takes place. The conservation of polarization under resonant Rayleigh scattering has been observed before [14,16]. In the second snapshot in Fig. 3 the total DCP of the momentum space image shows the largest positive value and the scattering ring is dominated by a positive DCP, which also extends into the middle of the scattering ring due to the energy loss through ongoing scattering processes. The main features of the typical OSHE pattern during the pseudospin precession still remain. The last snapshot in Fig. 3 shows a rather finely segmented picture where points of similar DCP are spread more widely in momentum space. Over the further course of the scattered beam this behavior stays the same until the intensity is too low to calculate reliable DCP values.

IV. THEORY

Within the pseudospin formalism the polarization of microcavity polaritons is characterized by the three-component pseudospin vector $\mathbf{S} = (S_x, S_y, S_z)$, where $S_{x,y,z}$ describe the intensities of the linear (collinear with the original coordinate basis axes components and the diagonal/antidiagonal ones) and circular polarization components, respectively. It directly maps to the conventional Stokes vector characterizing the polarization of the emitted light.

The evolution of the pseudospin in the scattered state $\mathbf{S_k} \equiv \mathbf{S_k}(t)$ characterized by the wave vector $\mathbf{k}$ can be described by the precession equation [17,18,26]

$$\frac{\partial \mathbf{S_k}}{\partial t} = \mathbf{S_k} \times \Omega_\mathbf{k} + \mathbf{f}(t) - \frac{\mathbf{S_k}}{\tau} \tag{2}$$

accompanied by the rate equation for the population of the considered state:

$$\frac{\partial N_\mathbf{k}}{\partial t} = f(t) - \frac{N_\mathbf{k}}{\tau}. \tag{3}$$

The vector $\Omega_\mathbf{k} = (\Omega_x, \Omega_y, \Omega_z)$ in the first term in the right-hand side of Eq. (2) describes the effective magnetic field causing oscillatory dynamics of the polariton pseudospin components. In our model, the effective magnetic field represents a combination of three fields of different origin:

$$\Omega_\mathbf{k} = \Omega_\mathbf{k}^{\mathrm{LT}} + \Omega_\mathbf{k}^{\mathrm{an}} + \Omega_\mathbf{k}^{\mathrm{NL}}. \tag{4}$$

The LT field $\Omega_\mathbf{k}^{\mathrm{LT}}$ describes the effect of the LT splitting of the linear polarizations and is given by

$$\Omega_\mathbf{k}^{\mathrm{LT}} = \left[\Delta_{\mathrm{LT}}\left(k_x^2 - k_y^2\right), 2\Delta_{\mathrm{LT}} k_x k_y, 0\right], \tag{5}$$

where Δ_{LT} is the LT-splitting constant and $k_{x,y}$ are the components of the wave vector characterizing the considered pseudospin state. This splitting is mostly governed by the TE-TM splitting of the photonic microcavity mode [27] along with the long-range electron and hole exchange interaction [28]. It is evident from Eq. (5) that the contribution of this field to the pseudospin dynamics is stronger the larger the absolute value of the wave vector $\mathbf{k}$ is.

The uniform effective field $\Omega_\mathbf{k}^{\mathrm{an}} = [\delta_{\mathrm{an}}, 0, 0]$ characterizes the effect of the built-in anisotropy splitting arising from the optical and electronic anisotropy in the microcavity [20,29]. It is worth noting that the magnitude of this splitting is $\mathbf{k}$ independent.

While both $\Omega_\mathbf{k}^{\mathrm{LT}}$ and $\Omega_\mathbf{k}^{\mathrm{an}}$ affect the linear polarization components of $\mathbf{S_k}$ in the cavity plane, the third effective magnetic field component, $\Omega_\mathbf{k}^{\mathrm{NL}} = [0, 0, \beta S_z]$, oriented in the growth direction plays the role of the effective Zeeman splitting of the circularly polarized polariton states. It emerges in Eq. (2) to characterize nonlinear effects during the polariton propagation. Since the polaritons are excited resonantly, the dominant sources of nonlinearity are polariton-polariton interactions. Accordingly, the effective field $\Omega_\mathbf{k}^{\mathrm{NL}}$ describes the so-called self-induced Larmor precession of the polariton pseudospin [30,31]. The parameter β is the effective polariton-polariton interaction constant that takes into account the difference of the exchange interaction strengths between two polariton states in the triplet configuration (parallel spins) and the singlet configuration (opposite spins).

The second term on the right-hand side of Eq. (2) describes the inflow of polaritons to the state $\mathbf{S_k}$. Hereafter we shall account only for the elastic (Rayleigh) scattering of polaritons. We consider the originally studied configuration of the OSHE [17] neglecting multiple scattering effects and assume the state $\mathbf{S_k}$ to be fed due to the scattering from the initial state $\mathbf{k}_0$ with $|\mathbf{k}_0| = |\mathbf{k}| = k$. Within this model, the polariton flux is found as [17,22]

$$\mathbf{f}(t) = 2\frac{\mathbf{S_{k0}}}{\tau_1} e^{-t/\tau}, \quad f(t) = 2\frac{S_{\mathbf{k}0}}{\tau_1} e^{-t/\tau}, \tag{6}$$

where τ_1 is the scattering time describing the scattering of polaritons from the initial state $\mathbf{k}_0$ to the state $\mathbf{k}$. $\mathbf{S_{k0}}$ is the pseudospin of the initial state, $S_{\mathbf{k}0} = |\mathbf{S_{k0}}|$. The temporal evolution of the initial state can be found from the equation $\partial \mathbf{S_{k0}}/\partial t = \mathbf{S_{k0}} \times \Omega_{\mathbf{k}0}$, where the time dependence of the nonlinear component of the effective magnetic field, $\Omega_{\mathbf{k}0}^{\mathrm{NL}}$, is taken into account in the explicit form.

The last terms in both Eqs. (2) and (3) describe the radiative relaxation due to the finite polariton lifetime τ in a given state.

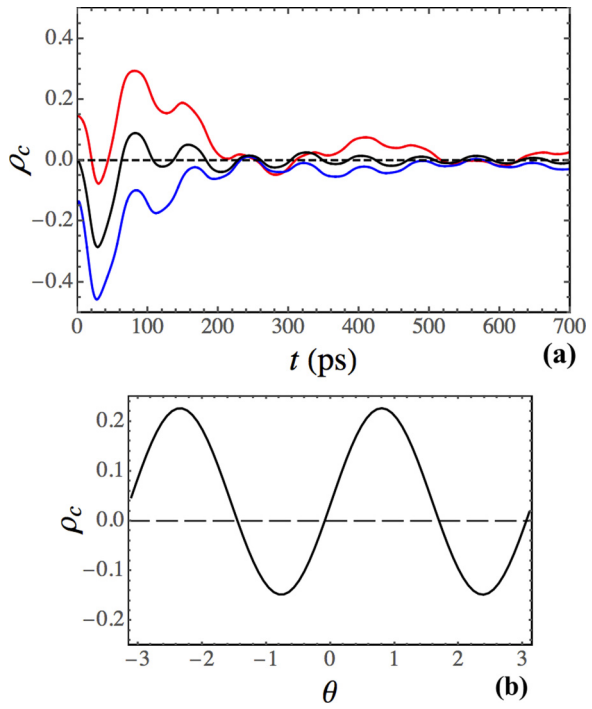

FIG. 4. (a) Theoretical prediction of the time evolution of the DCP of the two polariton polarization states at angles of $+45^\circ$ (the red curve) and -45° (the blue curve) with respect to the direction of the pump. The solid black curve corresponds to the total DCP integrated over the elastic circle with $k = 0.73\,\mu\text{m}^{-1}$. (b) Integrated DCP against the scattering angle θ. The parameters used for modeling are as follows: The LT splitting constant is $\hbar\Delta_{\text{LT}} = 18\,\mu\text{eV}\,\mu\text{m}^2$, the anisotropy splitting is $\hbar\delta_{\text{an}} = 15\,\mu\text{eV}$, and the effective interaction strength is $\hbar\beta = -0.45\,\text{meV}\,\mu\text{m}^2$. The lifetime of polaritons is $\tau = 5$ ps and the scattering time is $\tau_1 = 40$ ps.

Figure 4(a) demonstrates the time evolution of the DCP of the two polariton polarization states corresponding to those in Fig. 2(b). The scattered state wave-vector components are $k_x = k/\sqrt{2}$ and $k_y = \pm k/\sqrt{2}$ ("+" and "−" correspond to the two observed states scattered at $+45^\circ$ and -45° with respect to the direction of the pump). Both the DCP dynamics observed in Fig. 2(b) and predicted in Fig. 4(a) differ significantly from that calculated in Ref. [17] where the temporal dependencies of the DCP for the signal scattered at $+45^\circ$ and -45° are characterized by symmetric oscillations with a constant frequency which decay with some characteristic time. This discrepancy arises due to the different geometry and initial conditions of our experiment with respect to Refs. [17,18]. In particular, we need to take into account a slight ellipticity of the pump as follows: $S_{\mathbf{k}0,x}(0) = -0.9$, $S_{\mathbf{k}0,y}(0) = (1 - S^2_{\mathbf{k}0,x})^{-1/2}$, and $S_{\mathbf{k}0,z}(0) = 0$. The ellipticity is caused by the optical setup we have used. In addition, in our case the DCP is not zero at the beginning of the observed time frame. By choosing the initial conditions $\mathbf{S}_{\mathbf{k}}(0)$ that are fitting parameters of the model one can achieve a better agreement between the modeling results and the experimental data.

According to Fig. 4(a), the DCP undergoes oscillatory dynamics, from which one can distinguish two kinds of oscillations. The slower oscillations with a period of about 300 ps originate from the pseudospin precession around the effective magnetic field with the oscillation frequency given by $\Omega = |\Omega_{\mathbf{k}}|$. The fast ones with a period of about 70–80 ps are caused by the mismatch of the oscillation frequencies of the scattered state and the pump state due to the nonlinear effect of polariton-polariton interactions.

Figure 4(b) shows the time-averaged distribution of the DCP around the elastic circle corresponding to the incident pump wave vector $\mathbf{k}_0$. The dependence of the DCP on the scattering angle θ demonstrates a periodic character. However, in contrast to the predictions of Ref. [17], the positions of the maxima are shifted with respect to the zero-angle direction, $\theta = 0$, which manifests the rotation of the DCP distribution in the QW plane. Another interesting difference is that the distribution is biased towards positive values of the DCP. The origin of both effects can be traced back to the impact of the z component of the effective magnetic field induced by the spin-dependent polariton-polariton interactions. A similar contribution of the z component to the DCP distribution has been predicted theoretically in Ref. [22] for an external magnetic field applied normal to the cavity plane.

V. CONCLUSION

We have experimentally demonstrated the time behavior of the OSHE. The observed process can be described within the framework of the pseudospin model developed assuming a single Rayleigh scattering act per propagating polariton and taking into account the effect of the self-induced Zeeman splitting of polariton states due to spin-dependent polariton-polariton interactions. The polariton pseudospin undergoes a characteristic precession around the effective magnetic fields of different origin that results in the oscillatory behavior of the DCP of emitted light.

ACKNOWLEDGMENTS

We gratefully acknowledge financial support by the Deutsche Forschungsgemeinschaft in the framework of the ICRC TRR 160 within Project No. B7. The Würzburg group acknowledges support by the Deutsche Forschungsgemeinschaft within Project No. SCHN1376-3.1. E.S. acknowledges support from the Russian Foundation for Basic Research Grant No. 16-32-60104. A.K. and E.S. acknowledge support from a Engineering and Physical Sciences Research Council Hybrid Polaritonics Programme grant. A.K. acknowledges partial support from the HORIZON 2020 RISE project CoExAn (Grant No. 644076). A.K. acknowledges support from the Russian Foundation for Basic Research Grant No. 15-52-12018.

[1] A. Amo, T. C. H. Liew, C. Adrados, R. Houdre, E. Giacobino, A. V. Kavokin, and A. Bramati, Nat. Photon **4**, 361 (2010).

[2] C. Leyder, T. C. H. Liew, A. V. Kavokin, I. A. Shelykh, M. Romanelli, J. P. Karr, E. Giacobino, and A. Bramati, Phys. Rev. Lett. **99**, 196402 (2007).

[3] D. Ballarini, M. De Giorgi, E. Cancellieri, R. Houdré, E. Giacobino, R. Cingolani, A. Bramati, G. Gigli, and D. Sanvitto, Nat. Commun. **4**, 1778 (2013).
[4] D. Sarkar, S. S. Gavrilov, M. Sich, J. H. Quilter, R. A. Bradley, N. A. Gippius, K. Guda, V. D. Kulakovskii, M. S. Skolnick, and D. N. Krizhanovskii, Phys. Rev. Lett. **105**, 216402 (2010).
[5] D. V. Vishnevsky, D. D. Solnyshkov, N. A. Gippius, and G. Malpuech, Phys. Rev. B **85**, 155328 (2012).
[6] C. Ouellet-Plamondon, G. Sallen, F. Morier-Genoud, D. Y. Oberli, M. T. Portella-Oberli, and B. Deveaud, Phys. Rev. B **93**, 085313 (2016).
[7] T. Freixanet, B. Sermage, A. Tiberj, and R. Planel, Phys. Rev. B **61**, 7233 (2000).
[8] C. Adrados, T. C. H. Liew, A. Amo, M. D. Martín, D. Sanvitto, C. Antón, E. Giacobino, A. Kavokin, A. Bramati, and L. Viña, Phys. Rev. Lett. **107**, 146402 (2011).
[9] E. Wertz, A. Amo, D. D. Solnyshkov, L. Ferrier, T. C. H. Liew, D. Sanvitto, P. Senellart, I. Sagnes, A. Lemaître, A. V. Kavokin, G. Malpuech, and J. Bloch, Phys. Rev. Lett. **109**, 216404 (2012).
[10] W. Langbein, I. Shelykh, D. Solnyshkov, G. Malpuech, Y. Rubo, and A. Kavokin, Phys. Rev. B **75**, 075323 (2007).
[11] J. Schmutzler, P. Lewandowski, M. Aßmann, D. Niemietz, S. Schumacher, M. Kamp, C. Schneider, S. Höfling, and M. Bayer, Phys. Rev. B **91**, 195308 (2015).
[12] D. Niemietz, J. Schmutzler, P. Lewandowski, K. Winkler, M. Aßmann, S. Schumacher, S. Brodbeck, M. Kamp, C. Schneider, S. Höfling, and M. Bayer, Phys. Rev. B **93**, 235301 (2016).
[13] M. Aßmann, F. Veit, M. Bayer, A. Löffler, S. Höfling, M. Kamp, and A. Forchel, Phys. Rev. B **85**, 155320 (2012).
[14] R. Houdre, C. Weisbuch, R. P. Stanley, U. Oesterle, and M. Ilegems, Phys. Rev. B **61**, R13333(R) (2000).
[15] W. Langbein and J. M. Hvam, Phys. Rev. Lett. **88**, 047401 (2002).
[16] T. Freixanet, B. Sermage, J. Bloch, J. Marzin, B. Gayral, and R. Planel, Physica E **7**, 676 (2000).
[17] A. Kavokin, G. Malpuech, and M. Glazov, Phys. Rev. Lett. **95**, 136601 (2005).
[18] C. Leyder, M. Romanelli, J. P. Karr, E. Giacobino, T. C. Liew, M. M. Glazov, A. V. Kavokin, G. Malpuech, and A. Bramati, Nat. Phys. **3**, 628 (2007).
[19] M. Maragkou, C. E. Richards, T. Ostatnický, A. J. D. Grundy, J. Zajac, M. Hugues, W. Langbein, and P. G. Lagoudakis, Opt. Lett. **36**, 1095 (2011).
[20] A. Amo, T. C. H. Liew, C. Adrados, E. Giacobino, A. V. Kavokin, and A. Bramati, Phys. Rev. B **80**, 165325 (2009).
[21] E. Kammann, T. C. H. Liew, H. Ohadi, P. Cilibrizzi, P. Tsotsis, Z. Hatzopoulos, P. G. Savvidis, A. V. Kavokin, and P. G. Lagoudakis, Phys. Rev. Lett. **109**, 036404 (2012).
[22] S. Morina, T. C. H. Liew, and I. A. Shelykh, Phys. Rev. B **88**, 035311 (2013).
[23] K. V. Kavokin, I. A. Shelykh, A. V. Kavokin, G. Malpuech, and P. Bigenwald, Phys. Rev. Lett. **92**, 017401 (2004).
[24] G. Nardin, T. K. Paraïso, R. Cerna, B. Pietka, Y. Léger, O. El Daif, F. Morier-Genoud, and B. Deveaud-Plédran, Appl. Phys. Lett. **94**, 181103 (2009).
[25] See Supplemental Material at http://link.aps.org/supplemental/10.1103/PhysRevB.96.075309 for a video of the pseudospin evolution in momentum space.
[26] M. M. Glazov and L. E. Golub, Phys. Rev. B **77**, 165341 (2008).
[27] G. Panzarini, L. C. Andreani, A. Armitage, D. Baxter, M. S. Skolnick, V. N. Astratov, J. S. Roberts, A. V. Kavokin, M. R. Vladimirova, and M. A. Kaliteevski, Phys. Rev. B **59**, 5082 (1999).
[28] M. Z. Maialle, E. A. de Andrada e Silva, and L. J. Sham, Phys. Rev. B **47**, 15776 (1993).
[29] M. M. Glazov and L. E. Golub, Phys. Rev. B **82**, 085315 (2010).
[30] H. Flayac, D. D. Solnyshkov, and G. Malpuech, New J. Phys. **14**, 085018 (2012).
[31] D. N. Krizhanovskii, D. Sanvitto, I. A. Shelykh, M. M. Glazov, G. Malpuech, D. D. Solnyshkov, A. Kavokin, S. Ceccarelli, M. S. Skolnick, and J. S. Roberts, Phys. Rev. B **73**, 073303 (2006).